Lattice thermal conductivity of bulk $PtTe_2$ and $PtSe_2$

Hamza A H Mohammed[1,2*], Daniel P Joubert[1] and G M Dongho Nguimdo[3]

[1]The National Institute for Theoretical Physics, School of Physics and Mandelstam Institute for Theoretical Physics, University of the Witwatersrand, Johannesburg, Wits 2050, South Africa.

[2]Department of Physics, Shendi University, Shendi, Sudan

[3]College of Graduate Studies, University of South Africa, Pretoria, Unisa 0003, South Africa

E-mail: hamzad00@gmail.com

Abstract. Thermoelectric devices can play a role in efficiently using available energy by converting heat produced by a wide range of devices into electricity. Low lattice thermal conductivity is a requirement for efficient thermoelectric devices and layered materials offer potential in reducing the lattice thermal conductivity perpendicular to the layers. We present density functional theory calculations of the structural and lattice thermal properties of layered platinum dichalcogenides $PtTe_2$ and $PtSe_2$ compounds in the CdI_2 structure, space group $P\bar{3}m1$. Phonon and elastic constants calculations confirm that the compounds are dynamically and mechanically stable. Lattice thermal conductivities were calculated within the single-mode relaxation-time approximation of the linearized phonon Boltzmann equation. We found that at the room temperature, the in-plane lattice thermal conductivities for $PtTe_2$ and $PtSe_2$ are 6.54 and 9.33 $Wm^{-1}K^{-1}$, while perpendicular to the plane they are 1.8 and 2.06 $Wm^{-1}K^{-1}$, respectively. The out-of-plane thermal conductivities confirm that further investigation of $PtTe_2$ and $PtSe_2$ as thermoelectric materials is necessary.

1. Introduction

Thermoelectricity is the simplest technology applicable for direct thermal-electrical energy conversion. Thermoelectric (TE) devices can directly convert heat to clean electricity or work in "reverse" as a heat pump, without any noise, hazardous liquids, or greenhouse-gas emissions [1]. To evaluate thermoelectric performance, the dimensionless figure of merit $ZT = \frac{S^2\sigma}{\kappa}T$ is often used. Here S is the Seebeck coefficient, σ is the electrical conductivity, κ is the total thermal conductivity which is a sum of lattice contribution (κ_L) and electronic contribution (κ_e), and T is the temperature. It is rare to have a large Seebeck coefficient and metallic conductivity simultaneously. The discovery of $NaCo_2O_4$, which is a metallic transition-metal oxide, had a great impact on the search for thermoelectric materials since it has both a relatively high conductivity and a large Seebeck coefficient [3]. Transition-metal dichalcogenides (MX_2, M = transition metal, X = chalcogen) with CdI_2 trigonal structure and space group $P\bar{3}m1$ (No. 164) have layers that are weakly bound by long range van der Waals forces. Intercalation of many molecular and atomic species has been achieved in these materials, and the impact on their structural, magnetic, and electronic properties have been characterized [4] and a few MX_2 compounds have been the focus of thermoelectric studies [5]. Transition metal dichalcogenides (TMDs) have attracted a lot of attention in recent years due to their various applications,

including electrocatalysis, optoelectronics, supercapacitors and batteries [6].
Recently, $PtTe_2$ was reported to be a Lorentz violating type-II Dirac semimetal [7]. Its sister compound $PtSe_2$ has also been predicted to be a type-II Dirac semimetal. So far experimental research in bulk $PtSe_2$ crystals has been limited due to the lack of high quality single crystals [8]. In this work we investigated the lattice thermal conductivity of $PtTe_2$ and $PtSe_2$ and found that they have promising thermoelectric properties because of their relatively small lattice thermal conductivity.

2. Computational details

All calculations in this work were performed using Density Functional Theory (DFT) with the projector-augmented wave (PAW) pseudopotential [9] approach as implemented in the VASP package [10]. The generalized gradient approximation (GGA) of Perdew, Burke and Ernzerhof (PBE) [11] and its modified form for solid materials, PBEsol [12], were used as exchange correlation approximations. We performed calculations using an energy cut-off of 520 eV which leads to a total energy tolerance of about 0.1 meV. For the integration over the BZ, a Γ-centered Monkhorst-pack grid [13] of 8×8×6 was found to be sufficient. Long range interactions important in TMD compounds are not accounted for in the PBE and PBEsol approximations. Since they are often approximated by van der Waals corrections, we examined the effects of vdW-D2 [14], vdW-D3 [15] and vdW-TS [16] van der Waals corrections in conjunction with a PBE exchange-correlation approximation in this study. A 3×3×3 supercell was used for displacive phonon calculations [17] and for solving the linearized lattice Boltzmann transport equation in the single mode relaxation time approximation [19] using the phonopy [18] and phono3py [19] packages, respectively. In the thermal conductivity calculation 1057 unique triplet displacements were included in the calculation of the scattering terms [19].

3. Results and discussion

3.1. Structural parameters

We first present the calculated total binding energy against the cell volume for the studied PtTe 2 and PtSe 2 under the PBEsol, vdW-D3, vdW-D2 and vdW-TS approximations in Figure 1 and Figure 2 respectively. The solid line shows a third order Murnaghan equation of state [20] fit to the calculated data. The fully optimized equilibrium lattice constants of $PtTe_2$ and $PtSe_2$ for different approximations compared with experimental data are listed in Table 2. We observe that the formation and cohesive energies are negative, indicating that the reaction leading to the formation of the $PtTe_2$ and $PtSe_2$ structures is exothermic, suggesting that structures can be formed from their constituent atoms [21]. The a and b lattice parameters, the in-layer structural parameters, show the least variation across the different approximations. The interlayer spacing, defined by the c lattice parameter, show the most variation. We note that PBEsol gives the best equilibrium structural parameters for the $PtTe_2$ and $PtSe_2$, when compared to experiment. This is surprising, since for other layered transition metal dichalcogenides, for example MoX_2 compounds [22], van der Waals corrections are important in the simulated search for reasonable interlayer spacings.

3.2. Elastic stability

Elastic constants of $PtTe_2$ and $PtSe_2$ were calculated in order to check the mechanical stability. $PtTe_2$ and $PtSe_2$ in the trigonal $P\bar{3}m1$ symmetry has eight independent elastic constants, shown in Table 2. The elastic constants in Table 2, satisfy all the Born stability criteria [25], which indicate that $PtTe_2$ and $PtSe_2$ compounds are mechanically stable. Voigt (V) and Reuss (R) approximations [26] tend to give upper and lower limits of the mechanical and thermodynamic properties of a material, respectively. It was shown by Hill that the Reuss moduli are always less than the Voigt moduli, and the true values are expected to lie between the two approximations

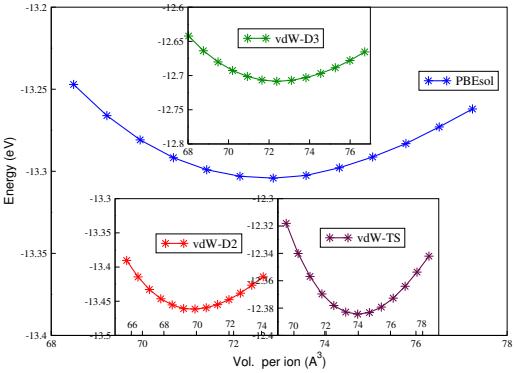

Figure 1. Calculated total binding energy versus cell volume, of $PtTe_2$ using PBEsol, vdW-D2, vdW-D3 and vdW-TS approximations.

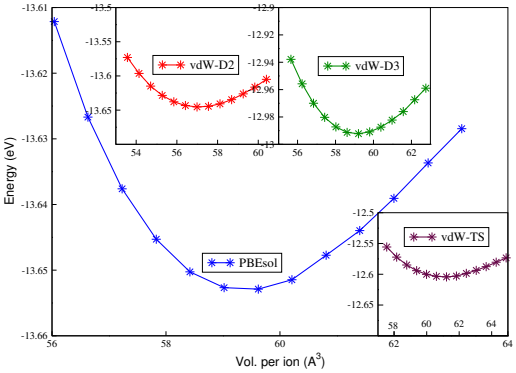

Figure 2. Calculated total binding energy versus cell volume, of $PtSe_2$ using PBEsol, vdW-D2, vdW-D3 and vdW-TS approximations.

Table 1. Calculated equilibrium lattice parameters, cohesive energy (E_{coh}) per atom and formation energy (E_{form}) per atom, bulk modulus B_0 (GPa), together with the experimental structural values of $PtTe_2$ and $PtSe_2$.

		$a = b$(Å)	c(Å)	V_o(Å^3)	E_{coh}(eV)	E_{form}(eV)	B_0(GPa)
$PtTe_2$							
	PBEsol	4.049	5.114	72.04	-4.43	-0.40	60
	vdW-D2	4.012	5.019	70.01	-4.48	-0.19	74
	vdW-D3	4.072	5.042	72.44	-4.23	-0.36	65
	vdW-TS	4.095	5.087	73.89	-4.13	-0.37	64
	Exp.[24]	4.010	5.201	72.43	—	—	—
$PtSe_2$							
	PBEsol	3.765	4.976	61.11	-4.55	-0.43	50
	vdW-D2	3.771	4.622	56.94	-4.55	-0.23	84
	vdW-D3	3.794	4.743	59.14	-4.33	-0.40	64
	vdW-TS	3.809	4.871	61.24	-4.20	-0.38	57
	Exp.[23]	3.727	5.081	61.15	—	—	—

[27]. Therefore, in this work, we consider the Hill method to derive the bulk modulus, elastic modulus and crystal elastic constant, as an average of the Voigt and Reuss values. Young's modulus (E) is the tendency of an object to deform along an axis when opposing forces are applied along that axis. Bulk moduli (B), describe the volumetric elastic tendency of an object to deform in all directions when uniformly loaded. We can loosely express it as an extension of Young's modulus in 3D. Shear moduli (G), describes the tendency of an object to shear (the deformation of shape at a constant volume) when acted upon by opposing forces. Poisson's ratio (ν), is associated with the nature of the atomic bonding. The values of bulk moduli obtained by the Birch equation of state shown in Table 2, is lower than that which are obtained by Hill approach shown in Table 2. The Young's moduli are higher than the bulk moduli and are similar to the Young's moduli of Silicon (Si) which is in range 133 - 188 GPa [28]. As stated before, Poisson's ratio (ν) provides information on bonding nature. Poisson's ratio for ionic bonding is

equal to or greater than $\nu = 0.25$ [29]. The calculated results of $\nu = 0.25 \sim 0.24$ for $PtTe_2$ and $PtSe_2$ suggest marginal ionic bonding.

Table 2. Elastic constants C_{ij} (GPa), elastic bulk moduli B_V(GPa), shear moduli G(GPa), Young's moduli E(GPa), Poisson's ratio and for of $PtTe_2$ and $PtSe_2$.

		C_{11}	C_{12}	C_{13}	C_{22}	C_{33}	C_{44}	C_{55}	C_{66}	B_V	E	G	ν
$PtTe_2$													
	PBEsol	170	53	42	170	67	45	45	58	68	105	42	0.24
	vdW-D2	200	62	55	200	83	65	65	68	84	129	52	0.24
	vdW-D3	175	52	48	175	77	49	49	61	74	111	44	0.25
	vdW-TS	169	52	42	169	69	42	42	58	68	103	41	0.24
$PtSe_2$													
	PBEsol	197	67	41	197	51	40	40	64	66	102	41	0.24
	vdW-D2	262	83	62	262	94	69	69	89	101	157	63	0.24
	vdW-D3	202	63	41	202	61	43	43	69	71	111	45	0.24
	vdW-TS	183	59	41	183	62	38	38	61	68	102	40	0.25

3.3. Dynamical stability

In order to test the dynamic stability of the $PtTe_2$ and $PtSe_2$, their underlying phonon dispersion relations were calculated. Since PBEsol gave the best lattice parameters, it was used in the computations of the phonon structure. The phonon band structure and density of states for $PtTe_2$ and $PtSe_2$ are presented in Figure 3 and Figure 4 respectively. The phonon frequencies are in the range of $0 - 6$ THz for $PtTe_2$ and $0 - 7$ THz for $PtSe_2$. The reduction in the range can be attributed to the relative atomic weights of Te and Se. All the phonon frequencies are positive, which indicates that the structure of $PtTe_2$ and $PtSe_2$ are dynamically stable, thereby satisfying one of the necessary conditions for crystal stability.

The primitive cell of $PtTe_2$ and $PtSe_2$ contains three atoms and therefore there are nine phonon modes for each wave vector, three acoustic modes and six optical modes. The highest frequencies of the acoustic modes, defined here as the acoustic cutoff, are approximately 3.44 THz and 4.58 THz for $PtTe_2$ and $PtSe_2$, respectively.

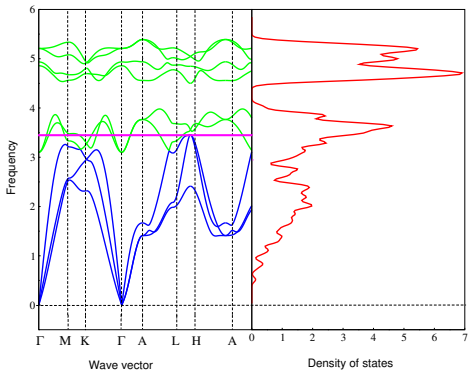

Figure 3. Phonon dispersion and DOS for $PtTe_2$.

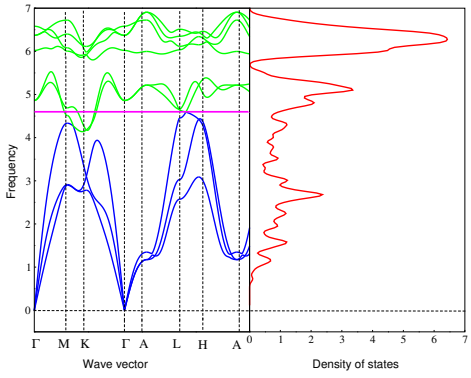

Figure 4. Phonon dispersion and DOS for $PtSe_2$.

3.4. Lattice thermal conductivity

The lattice thermal conductivity of $PtTe_2$ and $PtSe_2$ was calculated using the single-mode relaxation-time approximation to the linearized phonon Boltzmann equation [19]. The calculated lattice thermal conductivities of $PtTe_2$ and $PtSe_2$ in the range 0 to 1000 K are shown in Figure 5 and Figure 6 respectively, while the average of the cumulative thermal conductivities, as function of frequency at 300 K, are shown in Figure 7 and Figure 8 respectively. We note that the lattice thermal conductivity is highly anisotropic, with the thermal conductivity in the plane of the layers much higher than in the cross-plane direction.

Using Mattheissens rule [30] the average lattice thermal conductivity of $PtTe_2$ and $PtSe_2$ is 3.49, and 4.28 $Wm^{-1}K^{-1}$ respectively. The lattice thermal conductivities of these compounds is therefore small, which makes these compounds potential good thermoelectric materials.

We also estimated the contribution to the thermal conductivity from the acoustic modes at 300 K. We found that the in-plane acoustic mode contribution is 88.36% and 87.63% and cross-plane 71.34% and 68.00% for $PtTe_2$ and $PtSe_2$ respectively. This is in clear contrast to the conventional understanding, especially in the cross-plane direction, that the acoustic modes dominate thermal conductivity [30].

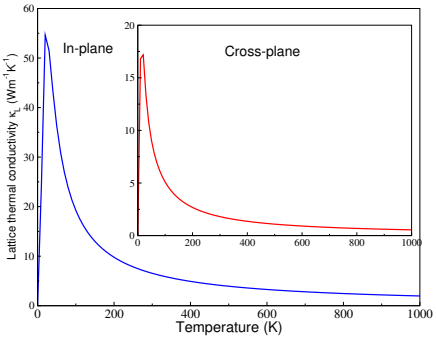

Figure 5. Lattice thermal conductivity Wm^{-1} K^{-1} $\kappa_L(T)$ for $PtTe_2$.

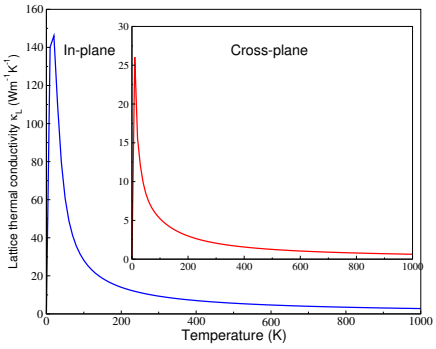

Figure 6. Lattice thermal conductivity Wm^{-1} K^{-1} $\kappa_L(T)$ for $PtSe_2$.

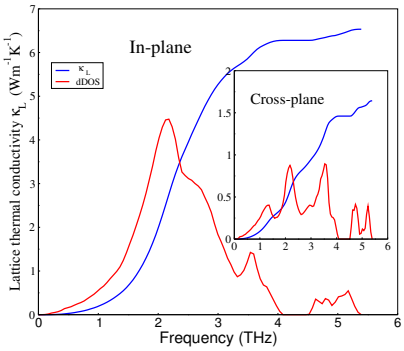

Figure 7. Average cumulative lattice thermal conductivity and derivative density $\kappa_L(\omega)$ for $PtTe_2$.

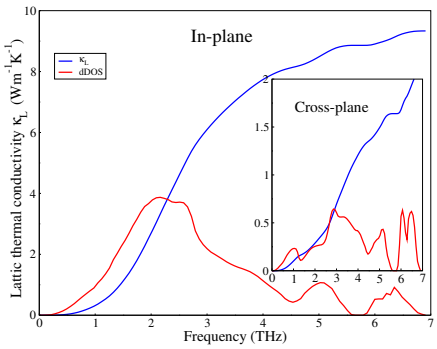

Figure 8. Average cumulative lattice thermal conductivity and derivative density $\kappa_L(\omega)$ for $PtSe_2$.

4. Conclusion

We have investigated the structural, mechanical and dynamical properties as well as the lattice thermal conductivity of bulk $PtTe_2$ and $PtSe_2$ from a first principles Density Functional Theory approach. Furthermore, we showed that the thermal conductivity of bulk $PtTe_2$ and $PtSe_2$ is highly anisotropic with the in-plane thermal conductivity much higher than the cross-plane thermal conductivity. The low value of the lattice thermal conductivity in the out-of-plane direction for both structures suggests that these materials are good candidates for thermoelectric applications.

Acknowledgements

We would like to acknowledge the financial support received from Shendi University, Shendi, Sudan. We also wish to acknowledge the Center for High Performance Computing (CHPC), Cape Town, South Africa, for providing us with computing facilities.

References

[1] Holgate T C, *et al* 2013 *J. Elec. Mater.* **42** 1751–1755.
[2] Mahan G D 1979 *Solid State Phys.* **51** 81–157.
[3] Terasaki I, Sasago Y and Uchinokura K 1997 *Phys. Rev. B.* **56** R12685.
[4] Yoffe A D 1983 *Solid State Ion.* **9** 59–69.
[5] Hor S and Cava J 2009 *Mater. Res. Bull.* **44** 1375–1378.
[6] Chen X, Wang M, Mo C and Lyu S 2015 *J. Phys. Chem. C* **119** 26706–26711.
[7] Yan M, *et al* 2017 *Nat. Commun.* **8** 257.
[8] Zhang K, *et al* 2017 *Phys. Rev. B* **96** 125102.
[9] Kresse G and Joubert D 1999 *Phys. Rev. B* **59** 1758.
[10] Kresse G and Furthmüller J 1996 *Comput. Mater. Sci.* **6** 15-50.
[11] Perdew P, Burke K and Ernzerhof M 1996 *Phys. Rev. Lett.* **77** 3865.
[12] Ruzsinsky A, Csonka G I and Vydrov O A 2008 *Phys. Rev. Lett.* **100** 136406.
[13] Monkhorst J and Pack D 1976 *Phys. Rev. B* **13** 5188.
[14] Bucko T, Hafner J, Lebegue S and Angyán J G 2010 *J. Phys. Chem. A* **114** 11814–11824.
[15] Moellmann J and Grimme S 2014 *J. Phys. Chem. C* **118** 7615–7621.
[16] Bučko T, Lebègue S, Ángyán J G and Hafner J 2014 *J. chem. phys.* **141** 034114.
[17] Togo A, Chaput L and Tanaka I 2015 *Phys. Rev. B* **91** 094306.
[18] Togo A, and Tanaka I 2015 http://phonopy. sourceforge. net.
[19] Togo A and Tanaka I 2015 *Scr. Mater.* **108** 1-5.
[20] Murnaghan D 1944 *Proc. Natl. Acad. Sci.* **30** 244–247.
[21] Lamfers J, Meetsma A, Wiegers A and De Boer L 1996 *J. Alloys Compd.* **241** 34–39.
[22] Zappa D 2017 *Materials.* **10** 1418.
[23] Furuseth S, Selte K and Kjekshus A 1965 *Acta Chem. Scand.* **19** 257.
[24] Thomassen L 1929 *J. Phys. Chem.* **2** 349–379.
[25] Mouhat F and Coudert X 2014 *Phys. Rev. B.* **90** 224104.
[26] Luo J and Stevens R 1996 *J. Appl. Phys.* **79** 9057–9063.
[27] Hill R 1952 *J. Proc. Phys. Soc.* **65** 349.
[28] Hopcroft M A, Nix W D and Kenny T W 2010 *J. Microelectromech. S* **19** 229–238.
[29] Bouhemadou A, *et al* 2009 *Comput. Mater. Sci.* **45** 474–479.
[30] Kittel C 2005 *Introduction to solid state physics* (USA: John Wiley and Sons, Inc).